# 3-Dimensional Analysis of Layer Structured Samples with High Depth Resolution Using Picosecond Laser-Induced Breakdown Spectroscopy

Rongxing Yi<sup>a,b</sup>, Dongye Zhao<sup>b\*</sup>, Jannis Oelmann<sup>b</sup>, Sebastijan Brezinsek<sup>b</sup>, Marcin Rasinski<sup>b</sup>, Matej Mayer<sup>c</sup>, Chandra Prakash Dhard<sup>d</sup>, Dirk Naujoks<sup>d</sup>, Liwei Liu<sup>a\*</sup>, Junle Qu<sup>a</sup> and the W7-X team<sup>e</sup>.

<sup>a</sup>Key Laboratory of Optoelectronic Devices and Systems of Guangdong Province, College of Physics and Optoelectronic Engineering, Shenzhen University, Shenzhen 518060, P. R. China.

<sup>b</sup>Forschungszentrum Jülich, Institut für Energie- und Klimaforschung - Plasmaphysik, Partner of the Trilateral Euregio Cluster (TEC), 52425 Jülich, Germany

<sup>c</sup>Max-Planck-Institut für Plasmaphysik, 85748 Garching, Germany

<sup>d</sup>Max-Planck-Institut für Plasmaphysik, 17491 Greifswald, Germany

<sup>e</sup>The W7-X Team are the co-authors mentioned in the paper, T. Klinger et al., Nuclear Fusion 59 (2019) 112004

**ABSTRACT:** 3-Dimensional (3D) analysis is crucial for many materials and can be used to study their structure and properties. Laser-Induced Breakdown Spectroscopy (LIBS) is a versatile tool to get depth information quickly but the poor depth resolution and (in general) a difficult quantification are the two main drawbacks. To solve these problems, a LIBS method based on picosecond-laser pulses is introduced. The ablation depth is measured and associated with the laser pulse number. A series of layer-structured graphite samples was tested by this method and the 2D and 3D layer structures of these samples were obtained with a resolution of up to 24 and 102 nm for Mo and C elements under a residual pressure of  $1 \times 10^{-5}$  Pa, respectively. This shows great potential of picosecond Laser-Induced Breakdown Spectroscopy (ps-LIBS) in the field of depth analysis.

#### Introduction

3D information (x, y and depth directions) is of great interest for many materials. It can be used to investigate the structure of the materials, to study the relationship between the structure and the performance of the materials in the field of functional material, and to study the processes of plasmamaterial interactions in the field of laser processing and nuclear fusion[1, 2]. Conventional methods which are used for obtaining the 2D or 3D elemental profile include: Scanning Electron Microscopy and Energy Dispersive X-ray spectroscopy (SEM/EDX), Scanning Electron Microscopy with Focused Ion Beam (SEM-FIB), Glow Discharge Optical Emission Spectrometry (GD-OES) and Elastic Backscattering Spectrometry (EBS). These methods are all classical methods and can be used to get useful information. However, SEM/EDX can't be applied to obtain depth information, SEM-FIB is powerful in depth analysis but time-consuming, GD-OES can provide high depth resolution but the lateral resolution is larger than 4 mm, EBS performs excellent in depth and good in lateral resolution (~1 mm) but the device is complicated and expensive. Above all, these methods have no or only small potential for in-situ analysis, which are their critical drawbacks.

Laser Induced Breakdown Spectroscopy (LIBS) is a spectrochemical analysis method based on analyzing spectra of plasmas generated by pulsed lasers. With its advantages of fast, remote detection, in-situ analysis ability and minimal sample preparation [3, 4], LIBS shows great potentials in many fields, such as on-line monitoring of steel [5-7], detection of heavy metals in environmental samples [8, 9], space exploration [10, 11] and nuclear fusion monitoring [12, 13]. Furthermore, LIBS can also be used to obtain the 3D elemental profile of materials due to the use of pulsed laser. Laser pulses can ablate the target layer by layer. By controlling the parameters and the scanning-path, 3D elemental profiles of the materials can be obtained by LIBS quickly.

It has been studied how to use LIBS to get the elemental distribution of different materials: the distribution of Li in lithium-ion batteries attracted much attention, they analyzed the lithium-ion batteries in air or in shielding gas and demonstrated the possibility of 3D elemental mapping of materials in lithium-ion batteries by LIBS [14, 15] with a depth resolution of hundreds of nanometers.

People in nuclear field studied how to detect solid depositions and gas (H and He) retention in wall materials (such as Mo, W, C) by LIBS in high vacuum [16-19]. However, most of the previous researches were limited to 1D or 2D analysis and they did not introduce layer structured samples for studying the 3D elemental distribution of the plasma facing materials by combining the laser ablation rate with the laser pulse number.

In this work, a method based on picosecond-LIBS (ps-LIBS) is introduced and applied to measure the depth information of a series of layer structured samples from Wendelstein7-X [20] (W7-X), one of the largest stellarators in the world, used for studying nuclear fusion. Layer structures and their quantitative depth information were observed under high vacuum conditions.

# **Experimental setup and sample**

Experimental setup: The LIBS experimental apparatus used in this study are schematically shown in figure 1. A picosecond laser (EKSPLA, PL2241, wavelength: 355 nm, repetition rate: 10 Hz, pulse width: 35 ps) was focused on the sample surface by a lens with a focal length of 500 mm. By focusing the laser beam to a diameter of 1 mm with a laser energy of 18 mJ, a laser energy density of 2.4 J cm<sup>-2</sup> was achieved. The samples were mounted onto a motorized XY\Φ translation stage. A vacuum chamber and a set of vacuum pumps were used to create a residual pressure of 1×10<sup>-5</sup> Pa to simulate the pressures in the W7-X plasma vessel. The plasma emission was coupled into an optical fiber by an optical lens and then collected by a USB spectrometer (Ocean Optics, HR2000, wavelength range: 350-800 nm, ungated). Meanwhile, a laser notch filter (wavelength range: 345-365 nm and 515-535 nm) was used to cut off the scattered laser.

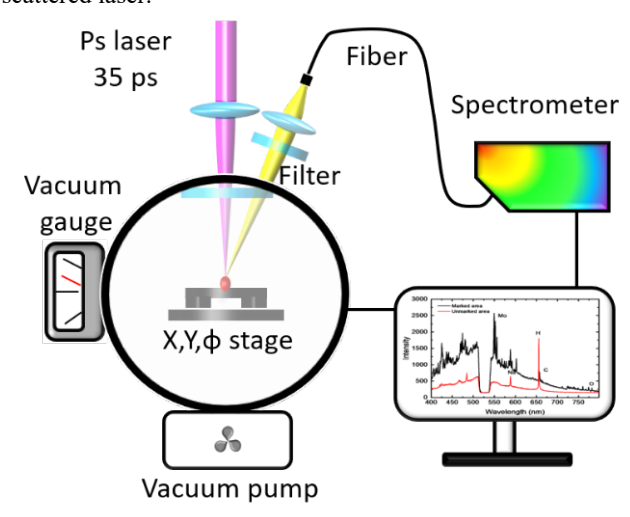


Figure 1. Ps-LIBS experimental setup.

**Samples:** In Figure 2 (a), the locations of the 2 target modules with marker layer stripes are shown from which the analyzed samples were retrieved. These tiles were exposed to H/He plasmas and removed at the end of the first operational phase in W7-X in divertor configuration. The technical names of the W7-X samples, have been simplified as A1-A5

and B1-B5. Samples A1-A5 are taken from the tile TM1v5 and B1-5 from TM2v2, the renaming is shown in table 1.

Figure 2 (b) shows the layer structure of the samples, the thickness of the top C layer ranges from 5-10 µm, the thickness of the thin pure Mo is around 200 nm. However, the profile of Mo layer is not a straight line, the thickness of the C/Mo coexistence layer is about 3.2 µm (distance between the two red dashed lines) in depth direction in this crater. After interaction with plasma in W7-X, erosions or depositions occurred in these samples. To study the erosion or depositions, 3-dimensional elemental information is very helpful, especially along the depth. As shown in Figure 2 (c), the sample with the marker layer stripe (stripe area 63×25 mm) was measured by LIBS with a laser crater of 1 mm. The distance between two craters was 5 mm. Measurements were done along the five lines, three on the marker layer stripe and two on the sides, each line contained 13-15 laser craters. In order to achieve depth resolved information about the material composition, 200 laser pulses were used for the subsequent ablation to ablate the whole marker layer and spectra recorded of every single ablation. Sample A1-A5 and B1-B5 were analyzed by this method.

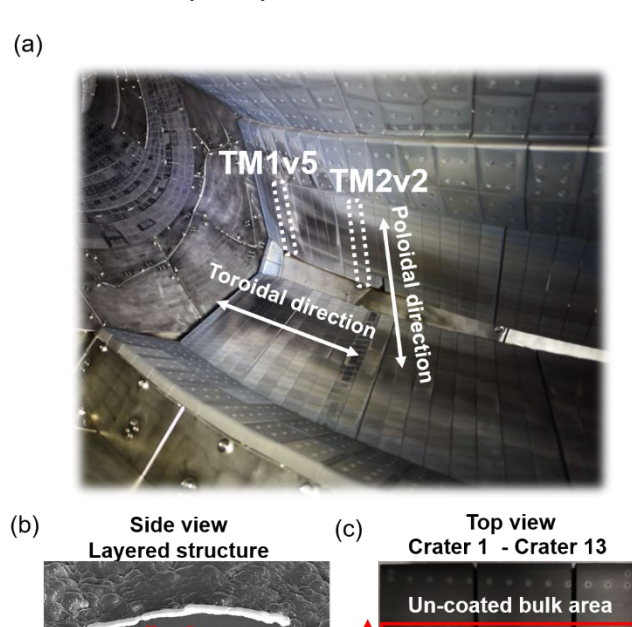


Figure 2. Sample measured by LIBS, (a) location of the samples, (b) layered structure of the sample, the top C layer is 5-10  $\mu$ m, the C/Mo coexistence layer is about 3.2 $\mu$ m (c) image of one sample and the laser craters.

Probe = 1000 pA | Name | 54.0° O1 | W7-K name = 46.75 pm | ND = 5.1 mm | 16.34 2010 | A603 p2

Table 1. Sample numbers of 2 tiles

Tile	Sample number

A	1	2	3	4	5
W7-X name (TM1v5)	A503	185	186	187	E503
В	1	2	3	4	5
W7-X name (TM2v2)	A603	191	192	193	E603

#### RESULTS AND DISCUSSION

Qualitative judgement of depth information: LIBS spectra of different laser pulses in the marker area are shown for a sample in figure 3. The signals of Mo, Na, H and C elements can be observed clearly. Obviously, the spectral intensities varied from pulse to pulse, especially for the Mo I line at 550.65 nm (marked by black dots box). In the spectrum of the 2<sup>nd</sup> laser pulse, Mo was not detectable in general due to the existence of the top C layer. After the graphite was ablated clearly by tens of laser pulses, the Mo signal appeared, as shown in the spectra of the 90<sup>th</sup> and 150<sup>th</sup> laser pulse. When the C/Mo coexistence layer was completely ablated, the Mo signal disappeared again, as shown in the last spectrum.

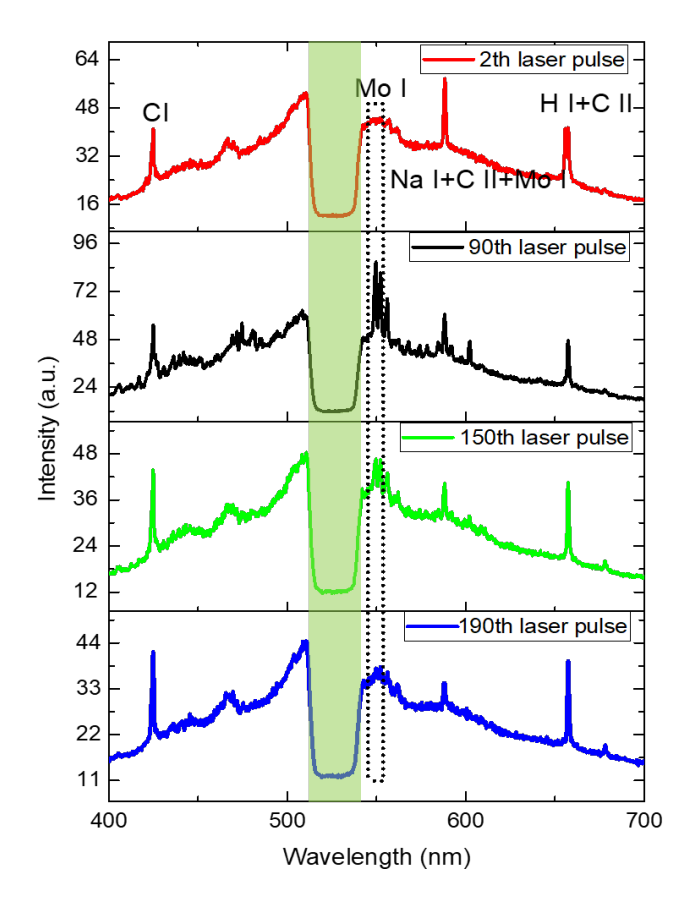


Figure 3. Typical spectra from one sample of the layered structure for different pulse number with Mo layer in marker area. The peaks of Mo, Na, H and C elements are observed. Due to a laser notch filter (532 nm laser filter), a dip appeared in the region from 515-535 nm.

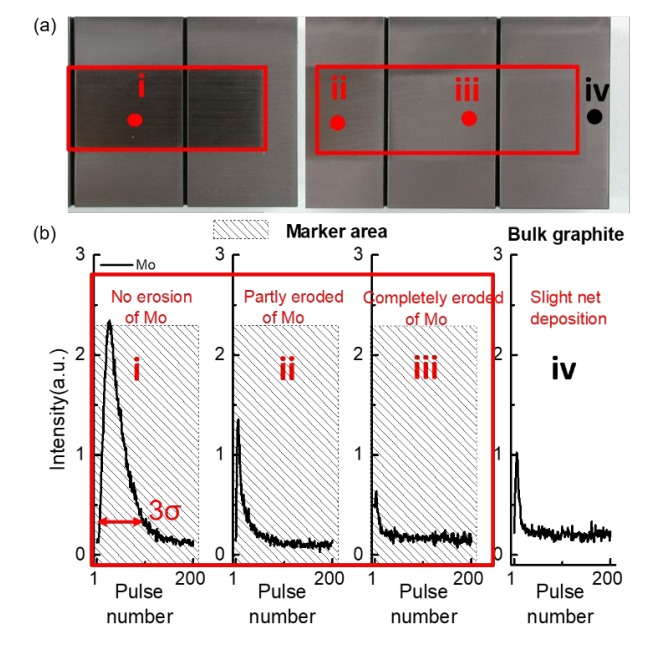


Figure 4. (a) The position of different craters and (b) corresponding intensities of Mo. For a judgement of erosion and deposition, the red arrow (3 $\sigma$ : 3 times noise of the spectrum) represents the background threshold of the signal. While the spectral intensity is higher than the line, it is considered as an effective signal. Position iv is outside of the initially coated area.

The variation of the spectral intensity of different laser pulses on a sample can provide useful depth resolved composition information. To get the depth resolved composition information in the present study, the relationship between pulse number and Mo spectral intensity is analysed in different samples. Figure 4 shows the Mo spectral intensity (Mo I at 550.65 nm) distribution in depth direction (different laser pulses), the data of 4 typical positions along the poloidal directions on the samples are presented. As shown in the upper part of figure 4 (a), position i represents the area without erosion of Mo (the top C layer was partly eroded), position ii represents the area with nearly half erosion of Mo, position iii represents the area where Mo was almost completely eroded and position iv represents the area without marker layer initially. The relationship between pulse number and Mo spectral intensity is shown in figure 4 (b). In position i, the Mo signal is observed for more than 90 laser pulses, the rising and falling of the Mo spectral intensity can be observed clearly, which meant there was an intact Mo layer. In position ii, the Mo signal was observed for about 30 laser pulses and the rising of the Mo spectral intensity disappeared, which indicated the C/Mo coexistence layer was partly eroded. In position iii, the Mo signal was observed for less than 10 laser pulses, which represented that almost the entire Mo layer was eroded. Finally, in position iv, the Mo signal was observed for several laser pulses, which meant a slight deposition of Mo occurred due to transport of eroded atoms.

Moreover, the depth of the Mo layer can be calculated qualitatively by the number of pulses during appearance and

disappearance of the effective Mo I signal (The LIBS signal is taken as effective signal, while the spectral intensity is higher than  $3\sigma$  of the spectrum. According to the formula LOD (Limit of Detection) = $3\sigma/k$ ,  $\sigma$  is the spectral noise and k is the slope of calibration curve, which means if the Mo concentration is higher than 1.7%, the LIBS signal is taken as effective). As shown in figure 4, data above the red arrow were regarded as the effective signal and the width of the peak correlated with the number pulses during the effective signal. The beginning and ending of effective signal represented the upper and lower surface of the C/Mo coexistence layer.

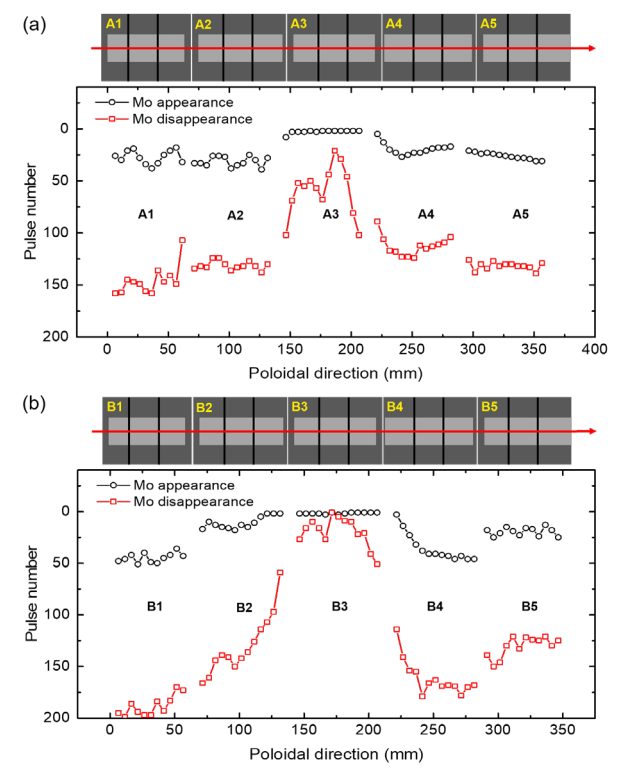


Figure 5. The Mo signal appearance (black hollow points) and disappearance laser pulse numbers (red hollow points) for different ablated craters on the series samples of (a) Tile A (1, 2, 3, 4, 5) and (b) Tile B (1, 2, 3, 4, 5), respectively. (The data come from the middle row in figure 2(c))

According to the measurement principle of effective signal and the relationship between pulse number and Mo spectral intensity, the beginning and ending of the effective signal of every laser crater on the marker layer was obtained. Figures 5 (a) and (b) show the appearance (black hollow points) and disappearance laser pulse numbers (red hollow points) of all the ablated craters in divertors from Tile A and Tile B, respectively. There was no signal of Mo before the laser pulse number of the black hollow point and after that of the red hollow point, which means no Mo element existed in the layer ablated by these laser pulses. Therefore, the thickness of the top C layer is related to the pulse number of the black hollow point, while the thickness of the C/Mo coexistence layer is related to the number of pulses between the black hollow point and the red hollow point.

As shown in figure 5, the thickness of the top C layer changed with the position on the sample. For the series samples of Tile A, compared to the areas in the middle, there was less erosion at both ends. On the left side, the thickness of the top C layer corresponded to about 20-40 "laser pulses" and the thickness of the C/Mo coexistence layer corresponded to about 100-130 "laser pulses" in these positions. However, erosion became more serious in the center of Tile A, the top C layer was practically eroded and the thinnest depth of the C/Mo coexistence layer corresponded to 24 "laser pulses". Compared with Tile A, erosion of Tile B was much more serious in the center area, not only the top C layer but also the C/Mo coexistence layer were entirely eroded in these positions, no Mo signal can be obtained even in the first few laser pulses

## Quantitative judgement of depth resolved information:

The above results showed the depth resolved information of Mo and C qualitatively, to obtain quantitative depth resolved information of the layers, ablation rates due to the same number of laser pulses for different elements were studied. Figure 6 (a) shows profiles of laser craters (60 pulses) of pure graphite, which was obtained by profilometer, the roughness (about  $2.1\mu m$ ) of the surface can be observed clearly. The ablation rate can be calculated by the laser pulse number and the ablation depth.

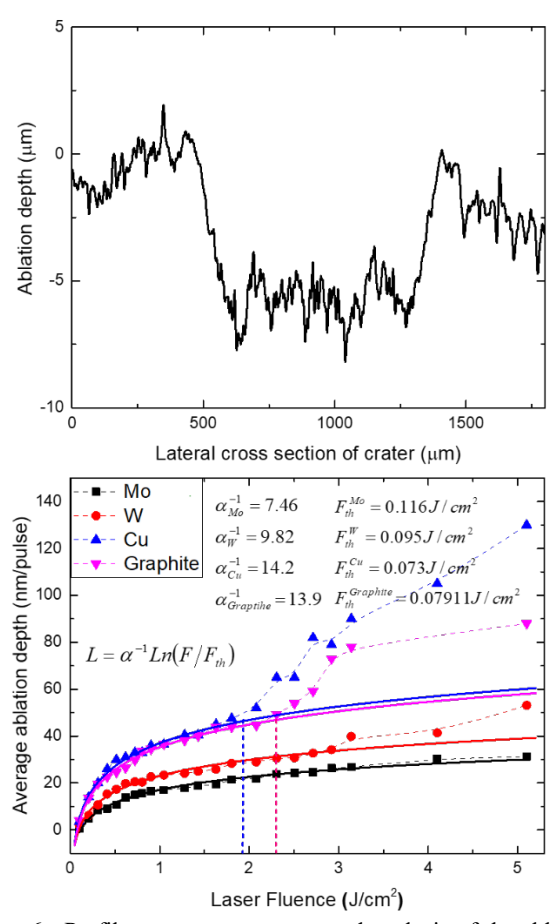


Figure 6. Profilometer measurement and analysis of the ablation depth for different laser fluences and materials. (a) Ablation profile of graphite sample obtained by profilometer. (b) Relationship between average ablation depth and laser fluence of different materials (relative error < 10%).

Ablation rates of 5 different materials (Mo, W, Cu, and fine grain graphite, all of them are bulk material with fine surfaces) are obtained by this method (100 pulses for each) are shown in table 2. Relationship between the calculated ablation rate of 5 materials and their laser fluences were analyzed, as shown in Figure 6 (b). The data matched well with log fit (when fluence is < 2.5J/cm<sup>2</sup> except Cu for which it is  $< 2J/cm^2$ . In the equation, L represents ablation rate,  $\alpha^{-1}$ is the optical penetration depth, Fth is the ablation threshold fluence and F is the real ablation fluence.), expected from ablation rate theory [21]. The different absorption efficiency, optical penetration depth [22] and boiling point lead to the distinctive ablation rate among these materials. The results show that the ablation rates of Mo and W were both lower than 40 nm/pulse under our experimental parameters. The ablation rate of graphite was a little higher, 102 nm/pulse. The ablation rate determines the depth resolution of our method, which indicated a best resolution of 24 nm for Mo element (laser fluence: 2.31 J/cm<sup>2</sup>).

Table 2. Ablation rate of different materials (laser fluence: 2.31 J/cm<sup>2</sup>)

Material	Mo	W	Cu	С
Ablation rate	24	30	64	102
(nm/pulse)				

By combining the ablation rate with the qualitative depth information (pulse number data in figure 5), quantitative depth of the marker area was obtained. Visualizations of the depth information of the top C layer and the C/Mo coexistence layer on Tile A and Tile B samples in poloidal direction are shown in figure 7. The gray area represents the thickness of the top C layer and the red area represents the thickness of the C/Mo coexistence layer (it should be clarified that the thickness of the C/Mo coexistence layer represents the distribution of Mo in depth direction. The depth which contains Mo is thicker than 3 µm, although the thickness of the pure Mo layer is only 200 nm, as shown in fig. 2(b).). These results consequently contained information in poloidal and depth direction, which makes this method a 2D analysis. Similar erosion results of graphite and Mo were obtained in the EBS results, both the results showed that the erosion dominated area locates in the B3 sample [23].

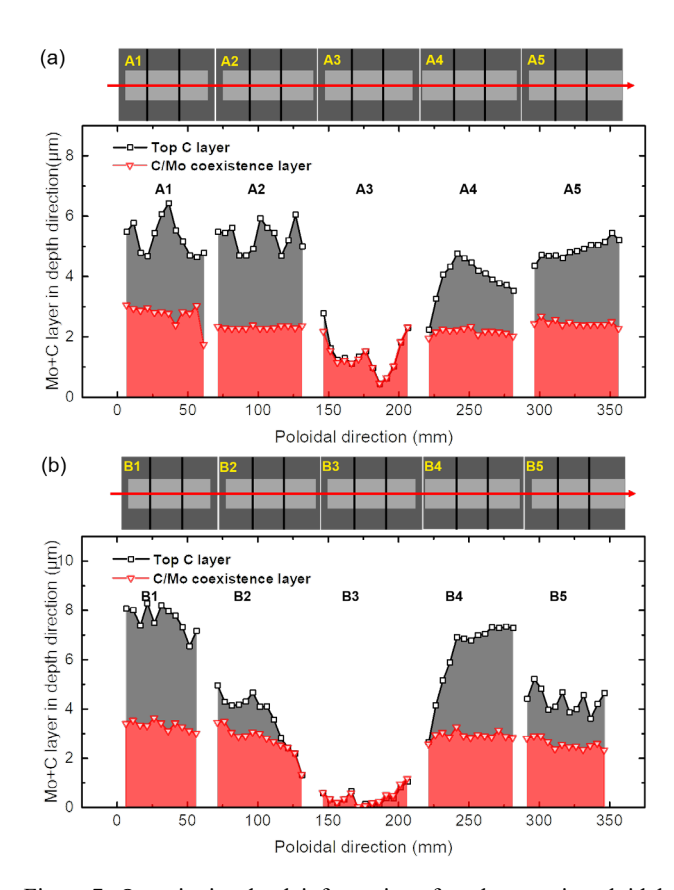


Figure 7. Quantitative depth information of marker area in poloidal direction of (a) Tile A (1, 2, 3, 4, 5) and (b) Tile B (1, 2, 3, 4, 5), respectively. The gray and the red area represent the approximate top C layer and the C/Mo coexistence layer, respectively.

Figure 8 shows depth information in poloidal and toroidal direction, which makes this method a 3D analysis. The selected sample was sample A3, which was eroded seriously in tile A. The marker area was about  $63 \times 25$  mm<sup>2</sup>, which contains  $13 \times 5 = 65$  craters. The depth of surrounding area was set as zero in fig. 8 as there was no marker layer. In sample A3, erosion of Mo almost appeared everywhere, only on the edge of the sample, some thin graphite layers remained.

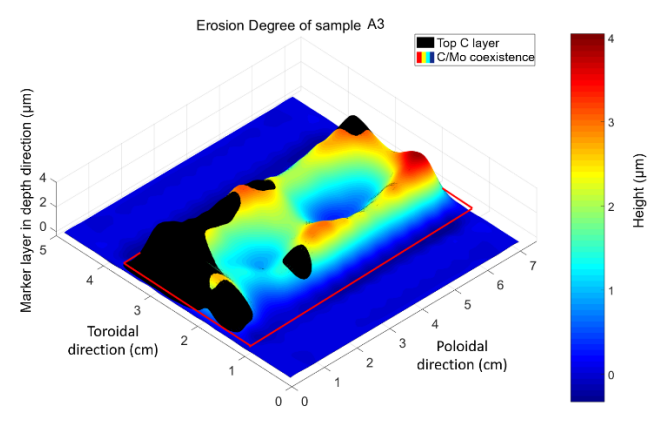
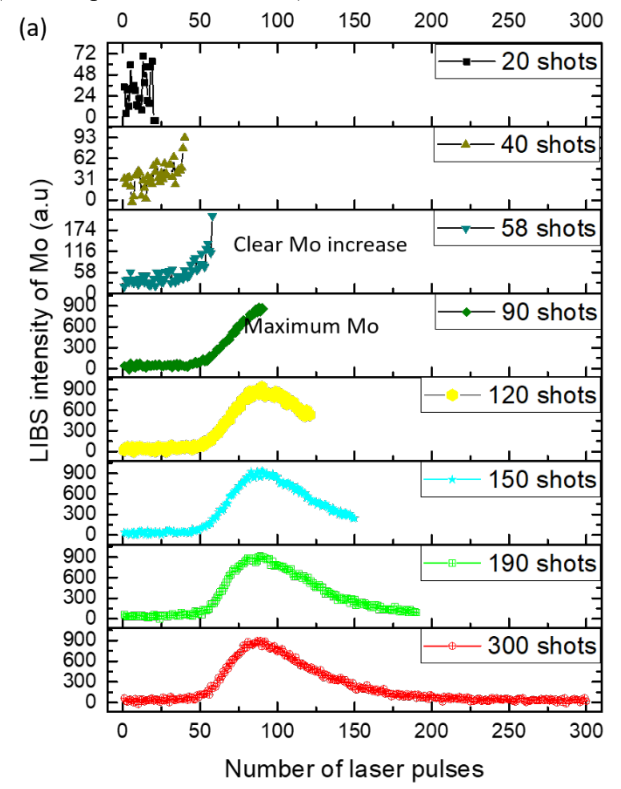


Figure 8. 3D elemental profile of sample A3 with a depth resolution of 23 nm. The marker area is marked by a red line. The black layer represents the remaining graphite layer.

Verification of the results of LIBS: Scanning Electron Microscope (SEM) and Energy Dispersive X-ray spectroscopy (EDX) were used to exam the results of LIBS. 8 points were ablated by different laser pulses in sample B1 (this sample was less eroded).



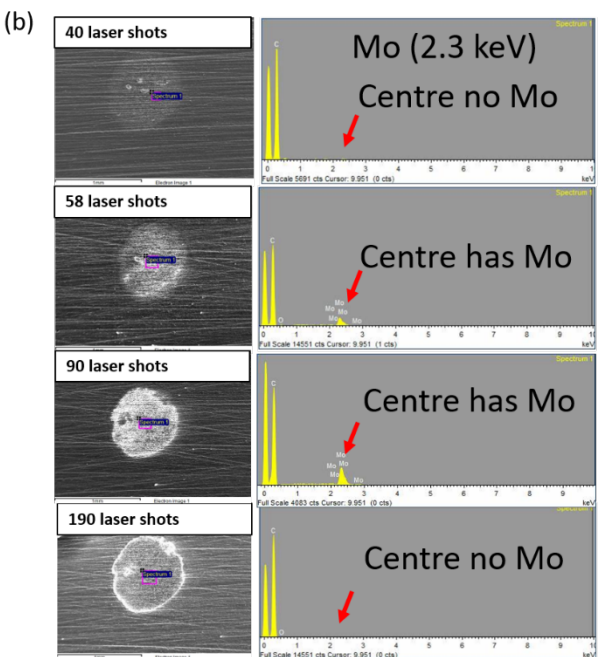


Figure 9. (a) Signal of Mo under different laser shots, (b) SEM images and EDX results of corresponding specific laser shots.

As shown in Figure 9 (a), there was no Mo signal in the first 40 laser pulses, after 58 pulses the Mo signal started to increase and reached its maximal value around 90 pulses. Then the Mo single decreased gradually until 190 pulses. Meanwhile, the SEM and EDX results verified the LIBS

spectrum. As shown in Figure 9 (b), no Mo signal was detected in craters of 40 and 190 laser pulses, while obvious Mo signal can be detected in craters of 58 and 90 laser pulses. The good agreement between LIBS results and SEM-EDX results shows the reliability of LIBS in 3D analysis for layer structure samples.

The 2D and 3D detection ability of LIBS has been verified in this work, its advantage of rapid and large area detection makes it more convenient when compared with FIB-SEM and EBS. Moreover, all the results were obtained under residual pressure of  $1 \times 10^{-5}$  Pa (used to simulate the pressures in W7-X), which shows its potential application of in-situ depth resolved analysis in W7-X. However, the low pressure is not indispensable, this method can be used in a normal ambient pressure as well, and a simpler setup can be obtained when the vacuum system is removed. The depth resolution is better than 100 nm for many elements, but the roughness of the sample influenced the depth resolution. To reduce this influence, a better lateral resolution is necessary. Therefore, to improve the performance of lateral resolution while maintaining the advantage of depth resolution is the key challenge of our future work.

## **CONCLUSIONS**

In this work, an analytical method based on ps-LIBS was proposed to 3D analysis of C/Mo layer structured samples with high depth resolution. Using this method, the C/Mo spectral intensities of different laser pulses were obtained and applied to determine the depth of the layer structured samples. The analyzed area was larger than 63× 25 mm² and the analyzed layer structured sample thickness was higher than 8 µm. Furthermore, the best depth resolutions of this method were 24 and 102 nm for Mo and C elements, respectively. This work opens up a new area for ps-LIBS to realize a high depth resolution and large area analysis of layer structured samples. It is believed that, with the improvement of the laser crater lateral resolution, the ps-LIBS method is promising for future in-situ high resolution 3D elemental profile analysis.

#### **AUTHOR INFORMATION**

# **Corresponding Author**

E-mail: do.zhao@fz-juelich.de, liulw@szu.edu.cn

#### Notes

The authors declare no competing financial interest.

#### **Author Contributions**

The manuscript was written through contributions of all authors. All authors have given approval to the final version of the manuscript.

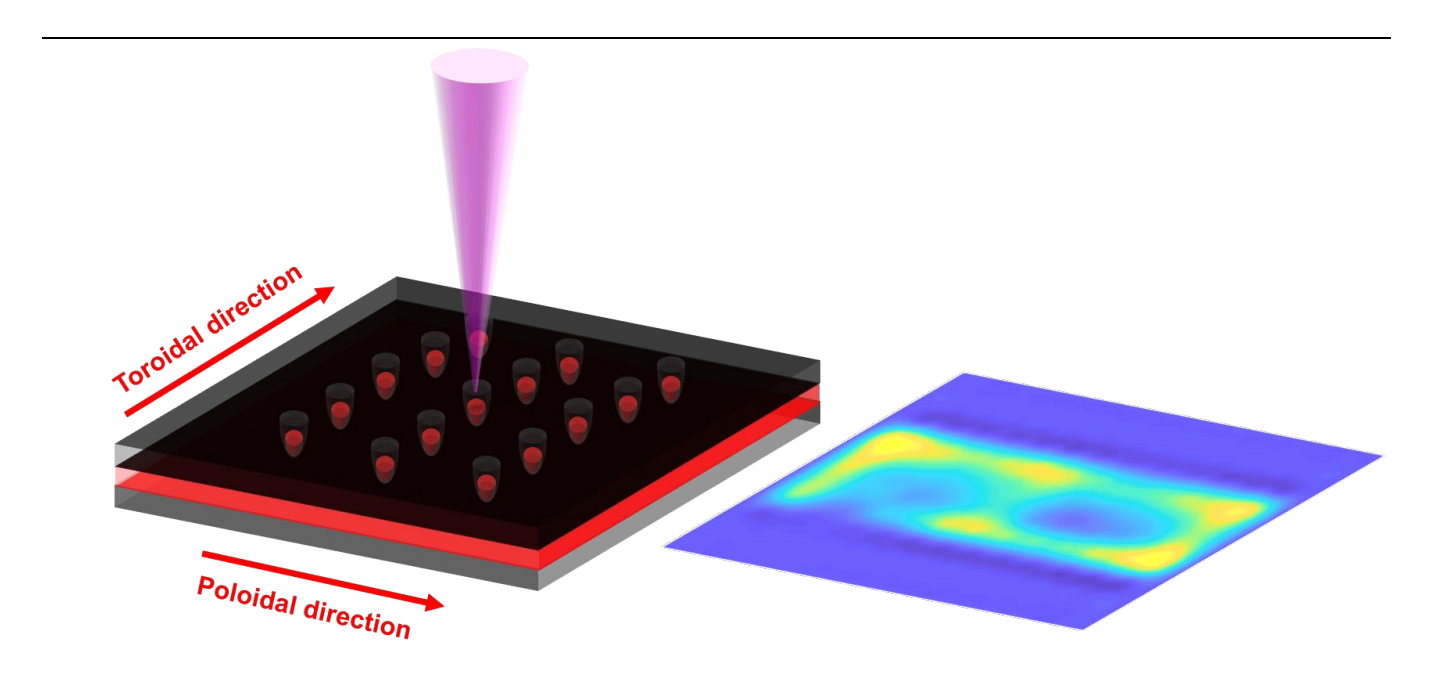
#### ACKNOWLEDGMENT

This work has been carried out within the framework of the EUROfusion Consortium and has received funding from the Euratom research and training programme 2014-2018 and 2019-2020 under grant agreement No 633053. The views and opinions expressed herein do not necessarily reflect those of the European Commission. This project is supported by The National Key Research and Development Program of China (2017YFA0700402). The National Natural Science Foundation of China (11904241/11905049/61722508/ 61525503/ 61620106016/ 81727804). Guangdong Natural Science Foundation Innovation Team (2014A030312008), Shenzhen Basic Research (JCYJ20150930104948169/ JCYJ20160328144746940/ GJHZ20160226202139185/ JCYJ20170412105003520). China Postdoctoral Science Foundation funded project 2018M643159. Project of Science and Technology Department of Sichuan Province (No. 20YYJC1703) and the Joint Sino-German Research Project (NSFC-DFG)

#### REFERENCES

- [1] J. Beuth, J. Fox, J. Gockel, C. Montgomery, R. Yang, H. Qiao, E. Soylemez, P. Reeseewatt, A. Anvari, S. Narra, Process mapping for qualification across multiple direct metal additive manufacturing processes, in: Proceedings of SFF Symposium., Austin, TX, Aug, 2013, pp. 12-14.
- [2] R. Montanari, B. Riccardi, R. Volterri, L. Bertamini, Characterisation of plasma sprayed W coatings on a CuCrZr alloy for nuclear fusion reactor applications, Materials Letters, 52 (2002) 100-105.
- [3] J.D. Winefordner, I.B. Gornushkin, T. Correll, E. Gibb, B.W. Smith, Comparing several atomic spectrometric methods to the super stars: special emphasis on laser induced breakdown spectrometry, LIBS, a future super star, Journal of Analytical Atomic Spectrometry, 19 (2004) 1061-1083.
- [4] Z. Wang, T.-B. Yuan, Z.-Y. Hou, W.-D. Zhou, J.-D. Lu, H.-B. Ding, X.-Y. Zeng, Laser-induced breakdown spectroscopy in China, Frontiers of Physics, 9 (2014) 419-438.
- [5] Z. Hao, L. Guo, C. Li, M. Shen, X. Zou, X. Li, Y. Lu, X. Zeng, Sensitivity improvement in the detection of V and Mn elements in steel using laser-induced breakdown spectroscopy with ring-magnet confinement, Journal of Analytical Atomic Spectrometry, 29 (2014) 2309-2314.
- [6] R. Noll, Laser-induced breakdown spectroscopy: fundamentals and applications, (2012).
- [7] X.H. Zou, L.B. Guo, M. Shen, X.Y. Li, Z.Q. Hao, Q.D. Zeng, Y.F. Lu, Z.M. Wang, X.Y. Zeng, Accuracy improvement of quantitative analysis in laser-induced breakdown spectroscopy using modified wavelet transform, Optics Express, 22 (2014) 10233-10238.
- [8] R. Yi, L. Guo, X. Zou, J. Li, Z. Hao, X. Yang, X. Li, X. Zeng, Y. Lu, Background removal in soil analysis using laser-induced breakdown spectroscopy combined with standard addition method, Optics Express, 24 (2016) 2607-2618.

- [9] R. Yi, J. Li, X. Yang, R. Zhou, H. Yu, Z. Hao, L. Guo, X. Li, X. Zeng, Y. Lu, Spectral interference elimination in soil analysis using laser-induced breakdown spectroscopy assisted by laser-induced fluorescence, Analytical chemistry, 89 (2017) 2334-2337.
- [10] D. Vaniman, M. Dyar, R. Wiens, A. Ollila, N. Lanza, J. Lasue, J. Rhodes, S. Clegg, H. Newsom, Ceramic ChemCam calibration targets on Mars science laboratory, Space science reviews, 170 (2012) 229-255.
- [11] A. Cousin, O. Forni, S. Maurice, O. Gasnault, C. Fabre, V. Sautter, R. Wiens, J. Mazoyer, Laser induced breakdown spectroscopy library for the Martian environment, Spectrochimica Acta Part B: Atomic Spectroscopy, 66 (2011) 805-814.
- [12] M.Z. Martin, S. Allman, D.J. Brice, R.C. Martin, N.O. Andre, Exploring laser-induced breakdown spectroscopy for nuclear materials analysis and in-situ applications, Spectrochimica Acta Part B: Atomic Spectroscopy, 74 (2012) 177-183.
- [13] R. Hai, P. Liu, D. Wu, Q. Xiao, L. Sun, H. Ding, Effect of steady magnetic field on laser-induced breakdown spectroscopic characterization of EAST-like wall materials, Journal of Nuclear Materials, 463 (2015) 927-930.
- [14] S. Imashuku, H. Taguchi, S. Fujieda, S. Suzuki, K. Wagatsuma, Three-dimensional lithium mapping of graphite anode using laser-induced breakdown spectroscopy, Electrochimica Acta, 293 (2019) 78-83.
- [15] H. Hou, L. Cheng, T. Richardson, G. Chen, M. Doeff, R. Zheng, R. Russo, V. Zorba, Three-dimensional elemental imaging of Li-ion solid-state electrolytes using fs-laser induced breakdown spectroscopy (LIBS), Journal of Analytical Atomic Spectrometry, 30 (2015) 2295-2302.
- [16] J. Oelmann, N. Gierse, C. Li, S. Brezinsek, M. Zlobinski, B. Turan, S. Haas, C. Linsmeier, Depth-resolved sample composition analysis using laser-induced ablation-quadrupole mass spectrometry and laser-induced breakdown spectroscopy, Spectrochimica Acta Part B: Atomic Spectroscopy, 144 (2018) 38-45.
- [17] A. Lang, D. Engelberg, N.T. Smith, D. Trivedi, O. Horsfall, A. Banford, P.A. Martin, P. Coffey, W.R. Bower, C. Walther, Analysis of contaminated nuclear plant steel by laser-induced breakdown spectroscopy, Journal of hazardous materials, 345 (2018) 114-122.
- [18] R. Hai, P. Liu, D. Wu, H. Ding, J. Wu, G.-N. Luo, Collinear double-pulse laser-induced breakdown spectroscopy as an in-situ diagnostic tool for wall composition in fusion devices, Fusion Engineering and Design, 89 (2014) 2435-2439.
- [19] G. Shaw, M. Bannister, T.M. Biewer, M.Z. Martin, F. Meyer, B.D. Wirth, The detection of He in tungsten following ion implantation by laser-induced breakdown spectroscopy, Applied Surface Science, 427 (2018) 695-703.
- [20] V. Winters, S. Brezinsek, F. Effenberg, M. Rasinski, O. Schmitz, L. Stephey, C. Biedermann, C. Dhard, H. Frerichs, J. Harris, Overview of the plasma-surface interaction on limiter surfaces in the startup campaign of Wendelstein 7-X, Physica Scripta, 2017 (2017) 014050.
- [21] R. Le Harzic, D. Breitling, M. Weikert, S. Sommer, C. Föhl, S. Valette, C. Donnet, E. Audouard, F. Dausinger, Pulse width and energy influence on laser micromachining of metals in a range of 100 fs to 5 ps, Applied Surface Science, 249 (2005) 322-331.
- [22] S. Preuss, A. Demchuk, M. Stuke, Sub-picosecond UV laser ablation of metals, Applied physics A, 61 (1995) 33-37.
- [23] M. Mayer, M. Balden, S. Brezinsek, V. Burwitz, C. Dhard, A. Dudek, G. Ehrke, Y. Gao, H. Greuner, R. Guimarães, Material erosion and deposition on the divertor of W7-X, Physica Scripta, 2020 (2020) 014035.



for TOC only